

Fe₃O₄@FSM-16-SO₃H as a new magnetically recyclable nanostructured catalyst: synthesis, characterization and catalytic application for the synthesis of pyrano[2,3-c]pyrazoles

Somayeh Hashemi-Uderji^a, Mohammad Abdollahi-Alibeik^{a,*}, Reza Ranjbar-Karimi^b

^aDepartment of Chemistry, Yazd University, Yazd 89158-13149, Iran.

^bDepartment of Chemistry, Faculty of Science, Vali-e-Asr University, Rafsanjan 77176, Iran.

Received 21 February 2018; received in revised form 10 September 2018; accepted 12 September 2018

ABSTRACT

A three-component process for the one-pot synthesis of 6-amino-4-aryl-5-cyano-3-methyl-1-phenyl-1,4-dihydropyrano[2,3-c]pyrazoles is described by the three-component reaction of aldehydes, 3-methyl-1-phenyl-1H-pyrazol-5(4H)-one and malononitrile in the presence of Fe₃O₄@FSM-16-SO₃H as an efficient magnetically recyclable mesoporous catalyst. Folded sheet mesoporous material (FSM-16) was prepared by intercalation of a layered, kanemite type sodium silicate with cetyltrimethylammonium (CTMA) ions in the presence of dispersed Fe₃O₄. The Fe₃O₄@FSM-16-SO₃H was synthesized by sulfonation of Fe₃O₄@FSM-16 and characterized by FESEM, XRD, BET, VSM and FT-IR techniques. This protocol suggests benefits in terms of higher yields and short reaction time. In addition, the catalyst could be separated using an external magnet and is reusable many times without any significant loss of activity.

Keywords: Magnetic nanoparticle, Fe₃O₄, FSM-16-SO₃H, Folded sheet mesoporous silica, Pyranopyrazoles, Recoverable catalyst, Heterogeneous.

1. Introduction

In recent years, the synthesis of superparamagnetic nanoparticles has been intensively extended for its basic scientific interest and many technological usages such as medical imaging [1], magnetic field assisted transport [2], separations and analyses [3]. Magnetic nanoparticles are particularly attractive because of other usages such as electronics [4], biotechnology [5], biomedicine [6], medicine [7], metal ion extraction [8], optical imaging [9], catalyst [10] and magneto resistance [11].

Among the magnetic compounds, iron oxide nanoparticles have been extensively investigated. This magnetic nanoparticle has been synthesized by precipitation [12], co-precipitation [13] and hydrothermal [14] methods.

Magnetic nanoparticles such as Fe₃O₄, can be applied as a core for the catalyst support in organic conversion [15]

because of efficient specifications such as easy recovery and pairing with organic ligands [16] and inorganic combinations such as silica [10]. Fe₃O₄ magnetite nanoparticle has been used as a core in the synthesis of many silica based mesoporous catalysts such as Fe₃O₄@MCM-41-NE₂-EDA-Cu [17], Fe₃O₄@B-MCM-41 [18], PCM-MN [19], Fe₃O₄@SBA-15 [20].

Among the mesoporous silica compounds, folded sheet mesoporous materials (FSM-16) are very notable compounds due to their high specific surface areas and pore volumes [21-27]. Chen and co-workers have studied the formation mechanism of the FSM-16 materials in detail [28]. FSM-16 materials are created through a folded sheet mechanism in which the condensation of the reactive silanol groups presented on the adjacent silicate layers in the CTMA kanemite complex leads to the formation of a hexagonal array of channels with the uniform pore size [22]. The acidic attributes of FSM-16 compounds and their usages in acid-catalyzed reactions have been reported [29,30].

Nowadays, substituted pyrano[2,3-c]pyrazoles are considered as remarkable compounds because of

*Corresponding author.

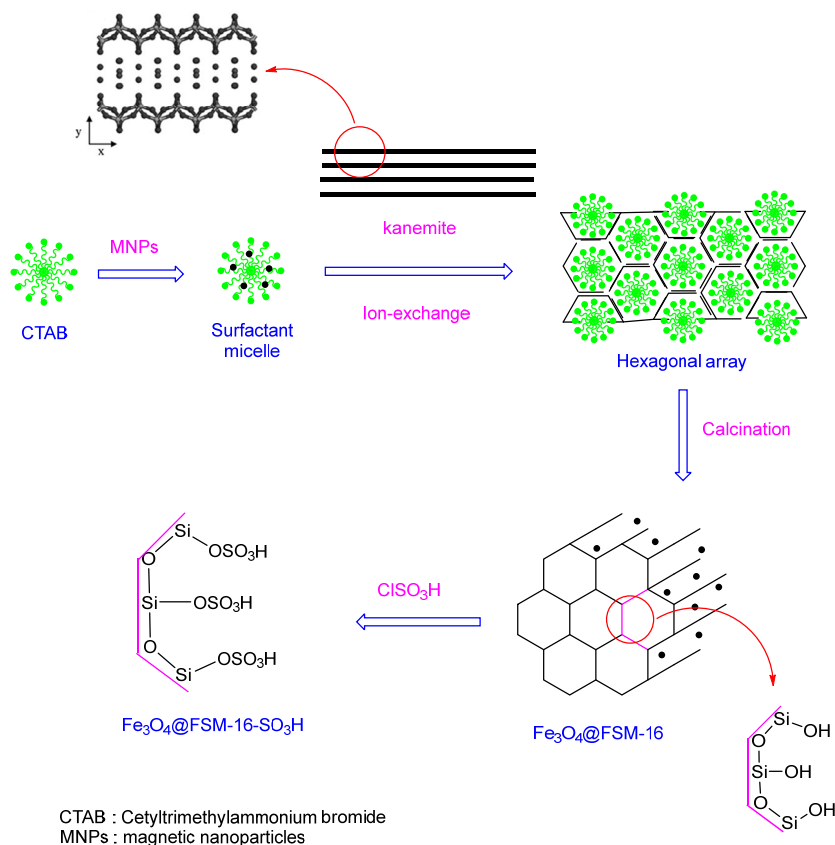
Email addresses: abdollahi@yazd.ac.ir, moabdollahi@gmail.com (M. Abdollahi-Alibeik)

pharmaceutical attributes. They represent a perfect range of biological activities including anti-inflammatory [31], antimicrobial [32], anticancer [33] activities and inhibitors of human Chk1 kinase [34]. The first synthetic procedure of this compounds was published by Junek et al. via the reaction of tetracyanoethylene and 3-methyl-1-phenylpyrazolin-5-one [35]. Another method for the synthesis of 6-amino-5-cyano-4-aryl-4H-pyrazolo[3,4-b]pyrans includes the reaction of arylidienemalononitrile with 3-methylpyrazoline-5-ones or the condensation of malononitrile and 4-arylidienepyrazoline-5-one [36]. Multi-component reaction (MCR) is one of the recent methods for the synthesis of fused pyran derivatives. The general method for the preparation of pyranopyrazole derivatives using a three-component

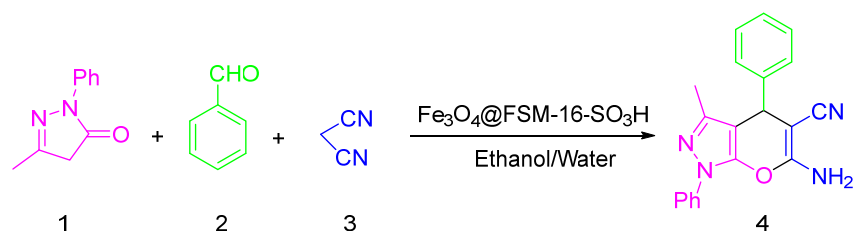
reaction is the reaction between pyrazolone, an aldehyde and malononitrile in the presence of diverse catalysts such as *p*-dodecylbenzene sulfonic acid (DBSA) [37], triethylbenzylammonium chloride (TEBA) [38], hexadecyltrimethylammonium bromide (HTMAB) [39], BF_3/MNPs [40], $\text{H}_{14}[\text{NaP}_5\text{W}_{30}\text{O}_{110}]$ [41], MgO [42] and $\text{KF}\cdot 2\text{H}_2\text{O}$ [43].

In this work, we aim to report the preparation and characterization of $\text{Fe}_3\text{O}_4@\text{FSM-16-SO}_3\text{H}$ as a new solid acid catalyst using kanemite as source of mesoporous silica (Scheme 1).

The catalytic activity of $\text{Fe}_3\text{O}_4@\text{FSM-16-SO}_3\text{H}$ was also studied in the reaction of various types of aldehydes, 3-methyl-1-phenyl-1H-pyrazol-5(4H)-one and malononitrile for the synthesis of pyrano[2,3-*c*]pyrazoles (Scheme 2).



Scheme 1. Schematic representation of the preparation of $\text{Fe}_3\text{O}_4@\text{FSM-16-SO}_3\text{H}$.



Scheme 2. Synthesis of pyrano[2,3-*c*]pyrazoles in the presence of $\text{Fe}_3\text{O}_4@\text{FSM-16-SO}_3\text{H}$

2. Experimental

2.1. Materials and methods

All materials were commercial reagent grade from Aldrich or Merck. All reaction progresses were monitored by TLC. The yields of products refer to isolated compounds. Melting points were achieved by a Buchi B-540 apparatus and are uncorrected. ^1H NMR and ^{13}C NMR spectra of pyranopyrazoles were recorded in DMSO- d_6 on a Bruker DRX-500 AVANCE spectrometer (400 MHz for ^1H and 100 MHz for ^{13}C). Infrared spectra of the reaction products and catalysts were obtained by a Bruker FT-IR Equinax-55 in KBr disks. The XRD patterns were obtained by a Bruker D8 ADVANCE X-ray diffractometer using Ni filtered Cu Ka radiation. Morphology of the catalyst was studied using a MIRA3TESCAN-XMU scanning electron microscope. The BET surface area was recorded on a micromeritics model ASAP2020 from the nitrogen adsorption-desorption isotherms at 77 K. All specimens were degassed at 120 °C under flowing nitrogen for 2 h. The specific surface area (S_{BET}) was achieved by the adsorption data using the BET equation, and the pore volume (V_{pore}) was estimated from the volume of adsorbed N_2 at the relative pressure (p/p^0) of 0.99. The pore size distribution was measured by the Barret-Joyner-Halenda (BJH) method. Potentiometric data was recorded using pH/mV meter, AZ model 86502-pH/ORP.

2.2. Preparation of magnetite nanoparticles (MNPs)

Magnetite (MNPs) was synthesized by the co-precipitation method. In a typical process, $\text{FeCl}_2 \cdot 4\text{H}_2\text{O}$ (1.99 g, 10 mmol) and $\text{FeCl}_3 \cdot 6\text{H}_2\text{O}$ (5.41 g, 20 mmol) were mixed in a round bottom flask containing 30 mL of distilled water. The mixture was heated to 60 °C under nitrogen with continuous stirring by a mechanical stirrer for 30 min. To this solution, 25% ammonia solution (35 mL) was added drop by drop with persistent stirring. The obtained black precipitate was stirred for about 30 min and then deposition was detached by an external magnet and washed with deionized water (3×100 mL) to remove the excess NH_3 . The gel was dried in an oven at 80 °C for 2 h.

2.3. Preparation of Fe_3O_4 @FSM-16 nanoparticles

To a solution of NaOH (3 g) dissolved in deionized water (30 mL), tetraethyl orthosilicate (16.6 mL) was added dropwise and then the mixture was stirred for 12 h at R.T. The solution was transferred into an oven and heated at 355 K for 4 h. The resulting

product was calcined at 923 K for 5 h to obtain $\delta\text{-Na}_2\text{Si}_2\text{O}_5$ (kanemite). The kanemite powder was deliquescent and immediately used for further treatment. Kanemite (5 g) was diffused in deionized water (50 mL) and then stirred for 3 h at 300 K. Then the suspension was filtered out to obtain wet kanemite paste. Fe_3O_4 nanoparticles (0.106 g, 0.457 mmol) were diffused in deionized water (40 mL) by ultrasound and cetyltrimethylammonium bromide (CTAB) (0.125 molL^{-1}) was added to this solution with the gentle increase of temperature to 343 K. To this suspension, the kanemite paste was added and then stirred at 343 K for 3 h. The pH value of the suspension was 11.5–12.5 at this stage. Afterwards, the pH value was adjusted carefully to 8.5 by adding 2 M hydrochloric acid with stirring. The suspension was kept under stirring at 343 K for 3 h keeping the pH value at 8–9. After cooling to room temperature, the solid product was separated by a centrifuge and then washed with distilled water (20 mL) and dried in oven at 393 K for 2 h to yield magnetite mesoporous silicate, Fe_3O_4 @FSM-16, with retaining the template. The product was calcined at 723 K to burn off the template to obtain final Fe_3O_4 @FSM-16.

2.4. Preparation of Fe_3O_4 @FSM-16- SO_3H nanoparticles

Magnetite FSM-16 (0.1 g) was placed in dry CH_2Cl_2 (2 mL) in a 5 mL round bottom flask equipped with a gas outlet tube and a dropping funnel containing a solution of chlorosulfonic acid (0.05 mL) in dry dichloromethane (1 mL). The chlorosulfonic acid solution was added drop-wise to the obtained suspension over a period of 30 min at room temperature. After the completion of the reaction, the sediment was separated by a centrifuge. The obtained brown solid was dried at 393 K in an oven for 2 h to obtain Fe_3O_4 @FSM-16- SO_3H .

2.4. General Experimental procedure for the synthesis of pyrano[2,3-*c*]pyrazoles

A mixture of aryl aldehyde (1 mmol), malononitrile (1 mmol), 3-methyl-1-phenyl-2-pyrazoline-5-one (1 mmol), and Fe_3O_4 @FSM-16- SO_3H (30 mg) was stirred in a mixture of water and ethanol (2 mL, 2:8) at reflux conditions. After completion, as it can be seen from TLC, the magnetic catalyst was removed from reaction mixture by an external magnet and washed with ethanol (2×3 mL). After evaporation of solvent, the crude products were crystallized from ethanol to give pure products (4a-l).

Selected spectral data

6-Amino-3-methyl-1,4-diphenyl-1,4-dihydropyrano[2,3-c]-pyrazole-5-carbonitrile (**4a**):

^1H NMR (400 MHz, DMSO- d_6): δ = 7.79 (d, J = 8.0 Hz, 2H), 7.50 (t, J = 8.0 Hz, 2H), 7.33–7.38(m, 3H), 7.25–7.29 (m, 3H), 7.23 (s, NH₂), 4.69 (s, 1H), 1.79 (s, 3H) ppm. ^{13}C NMR (100 MHz, DMSO- d_6): δ = 181.0, 159.4, 145.2, 143.6, 137.5, 129.3, 128.5, 127.8, 127.0, 126.1, 119.9, 109.5, 98.6, 58.1, 36.7, 12.5 ppm. FT-IR (KBr): $\bar{\nu}$ = 733, 1027, 1065, 1125, 1264, 1385, 1444, 1515, 1592, 2198, 3324, 3471 cm^{-1} .

6-Amino-3-methyl-4-(4-chlorophenyl)-1-phenyl-1,4-dihydropyrano[2,3-c]pyrazole-5-carbonitrile (**4b**):

^1H NMR (400 MHz, DMSO- d_6): δ = 7.79 (d, J = 8.0 Hz, 2H), 7.50 (t, J = 8.0 Hz, 2H), 7.42 (d, J = 8.0 Hz, 2H), 7.30–7.35 (m, 3H), 7.27 (s, NH₂), 4.74 (s, 1H), 1.80 (s, 3H) ppm. ^{13}C NMR (100 MHz, DMSO- d_6): δ = 188.0, 159.3, 145.2, 143.6, 137.5, 129.3, 128.5, 127.8, 127.7, 127.0, 126.1, 119.9, 98.6, 58.1, 36.7, 12.5 ppm. FT-IR (KBr): $\bar{\nu}$ = 3448, 3323, 2198, 1660, 1519, 1490, 1392, 1128, 756 cm^{-1} .

6-Amino-3-methyl-4-(3-nitrophenyl)-1-phenyl-1,4-dihydropyrano[2,3-c]pyrazole-5-carbonitrile (**4f**):

^1H NMR (400 MHz, DMSO- d_6): δ = 8.16–8.17 (m, 2H), 7.79 (m, 3H), 7.68 (t, 1H, J = 8.0 Hz), 7.51 (t, 2H, J = 8.0 Hz), 7.38 (s, NH₂), 7.34 (t, 1H, J = 8.0 Hz), 4.98 (s, 1H), 1.81 (s, 3H) ppm. ^{13}C NMR (100 MHz, DMSO- d_6): δ = 159.7, 147.9, 145.9, 145.1, 144.0, 137.4, 134.7, 130.3, 129.3, 126.3, 122.2, 120.1, 119.7, 97.6, 57.0, 36.1, 12.6 ppm. FT-IR (KBr): $\bar{\nu}$ = 3437, 3298, 2194, 1651, 1595, 1517, 1400, 1352, 1263, 1122, 1070, 756, 694 cm^{-1} .

6-Amino-3-methyl-4-(4-nitrophenyl)-1-phenyl-1,4-dihydropyrano[2,3-c]pyrazole-5-carbonitrile (**4k**):

^1H NMR (400 MHz, DMSO- d_6): δ = 8.24 (d, J = 8.8 Hz, 2H), 7.80 (d, J = 8.4 Hz, 2H), 7.59 (d, J = 8.8 Hz, 2H), 7.51 (t, J = 7.6 Hz, 2H), 7.40 (s, NH₂), 7.34 (t, J = 6.4, 1H), 4.94 (s, 1H), 1.80 (s, 3H) ppm. ^{13}C NMR (100 MHz, DMSO- d_6): δ = 181.4, 159.6, 151.2, 146.6, 145.1, 137.4, 129.3, 129.2, 126.3, 123.9, 120.1, 97.6, 66.6, 36.3, 12.5 ppm. FT-IR (KBr): $\bar{\nu}$ = 3338, 3213, 2191, 1666, 1595, 1517, 1402, 1350, 1132, 821 cm^{-1} .

3. Results and Discussion

3.1. Characterization of the catalyst

The FSM-16, Fe₃O₄@FSM-16 and Fe₃O₄@FSM-16-SO₃H were characterized by FT-IR, FESEM, XRD, and BET techniques.

The results of field emission scanning electron microscopy (FESEM), used to study the morphology and particle size of the catalysts, are shown in Fig. 1. The FESEM image of Fe₃O₄@FSM-16-SO₃H shows nanoparticles with spherical morphology in the range of < 100 nm.

To investigate the elemental composition of the Fe₃O₄@FSM-16-SO₃H, EDX analysis was done and results are shown in Fig. 2. Presence of the Fe and S related to the MNPs and -SO₃H functional groups are obvious (Table 1).

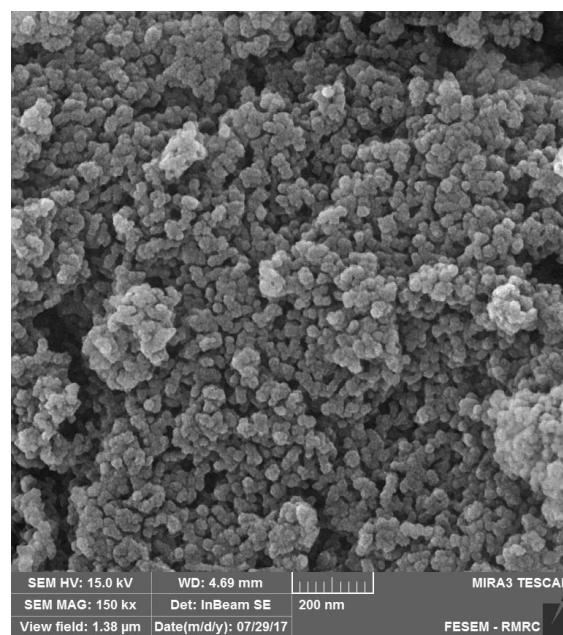


Fig. 1. FESEM images of Fe₃O₄@FSM-16-SO₃H.

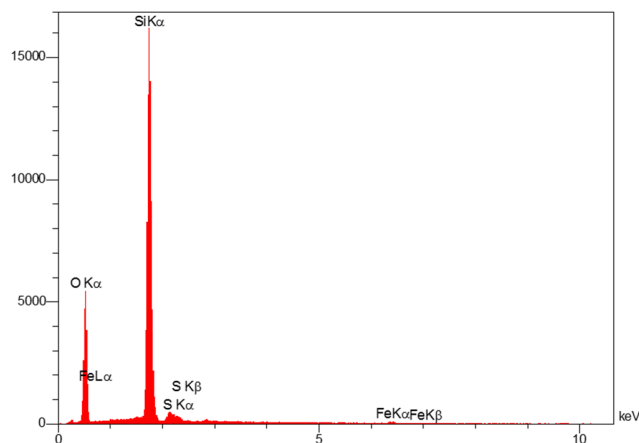


Fig. 2. Energy dispersive X-ray spectrum of Fe₃O₄@FSM-16-SO₃H.

Table 1. Elemental composition of Fe₃O₄@FSM-16-SO₃H.

Element	O	Si	S	Fe
Wt.%	56.96	41.14	1.26	0.64

The FT-IR spectra of Fe_3O_4 , FSM-16, $\text{Fe}_3\text{O}_4@\text{FSM-16}$ and $\text{Fe}_3\text{O}_4@\text{FSM-16-SO}_3\text{H}$ are presented in Fig. 3. The spectrum of FSM-16 (Fig. 3b) shows characteristic peaks at 1,205, 1,090, and 799 cm^{-1} relating to asymmetric and symmetric stretching vibrations of Si–O–Si and the peak of 966 cm^{-1} relating to Si–OH groups. The peak at 471 cm^{-1} is assigned to the bending vibration of Si–O–Si. The FT-IR spectrum of Fe_3O_4 is presented in Fig. 3a. The characteristic adsorption peak of Fe–O in the tetrahedral sites of magnetite nanoparticles is observed at 584 and 630 cm^{-1} [44]. For $\text{Fe}_3\text{O}_4@\text{FSM-16-SO}_3\text{H}$ (Fig. 3d), the peak of Fe–O bond is observed at 584 cm^{-1} that overlaps with the S–O stretching in 600 cm^{-1} . The increase in the intensity of main peak of FSM-16 (Si–O–Si peak) is the result of the overlap of asymmetric and symmetric stretching bands of SO_2 in 1120–1230 and 1010–1080 cm^{-1} , respectively, with Si–O–Si stretching bands in the region of 1000–1250 cm^{-1} (Fig. 3d).

The low angle XRD patterns of FSM-16, $\text{Fe}_3\text{O}_4@\text{FSM-16}$ and $\text{Fe}_3\text{O}_4@\text{FSM-16-SO}_3\text{H}$ are shown in Fig. 4. The characteristic peaks of FSM-16 (Fig. 4c) have appeared at $2\theta = 2.38^\circ$, 4.11° , and 4.73° , they were in accordance with the literature [45].

In the pattern of $\text{Fe}_3\text{O}_4@\text{FSM-16-SO}_3\text{H}$, the width of the main peak was increased and its intensity was decreased. This means that the hexagonal mesostructures are less ordered due to incorporation of magnetite nanoparticles and $-\text{SO}_3\text{H}$ groups into the network of FSM-16 (Fig. 4b).

The high angle XRD pattern of $\text{Fe}_3\text{O}_4@\text{FSM-16-SO}_3\text{H}$ (Fig. 5b) shows weak peaks at $2\theta = 30.3^\circ$, 35.6° , 43.3° , 53.8° , 57.4° and 62.9° corresponding to Fe_3O_4 nanoparticles (Fig. 5a) [18]. This result confirms that resulting Fe_3O_4 nanoparticles have pure single structures in cores.

The textural properties of $\text{Fe}_3\text{O}_4@\text{FSM-16-SO}_3\text{H}$ were studied by N_2 adsorption–desorption isotherm. Considering the results, the surface area (S_{BET}), pore volume (V_{pore}) and pore diameter (D_{pore}) of $\text{Fe}_3\text{O}_4@\text{FSM-16}$ are 842.6 m^2/g , 1.023 cm^3/g , and 4.86 nm respectively. A decrease in the surface area and pore volume in sulfonated samples is due to the adsorption of sulfonate on the inner surface of mesoporous channels. They are gathered in Table 2.

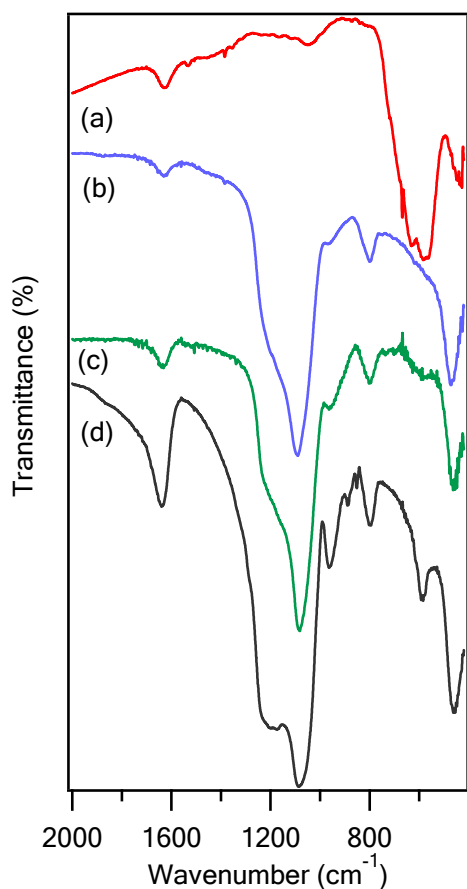


Fig. 3. FT-IR spectra of (a) Fe_3O_4 , (b) FSM-16, (c) $\text{Fe}_3\text{O}_4@\text{FSM-16}$, (d) $\text{Fe}_3\text{O}_4@\text{FSM-16-SO}_3\text{H}$.

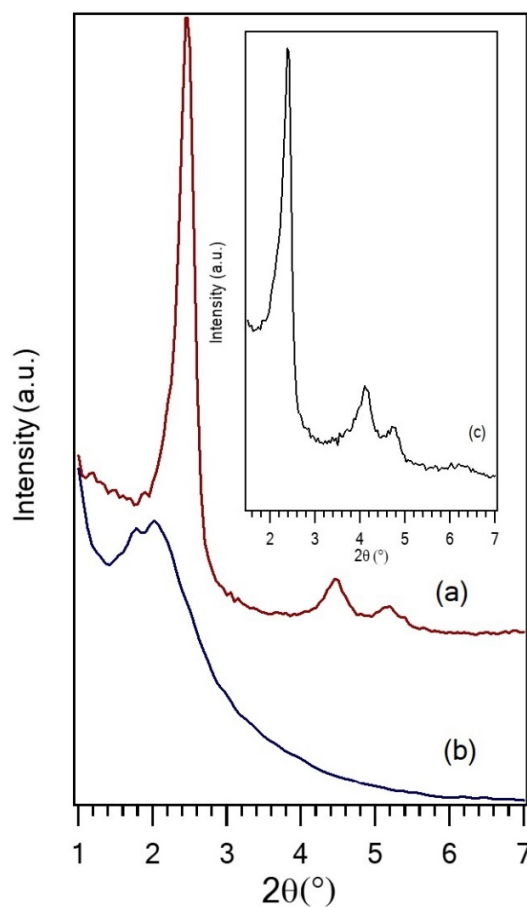


Fig. 4. Low angle XRD patterns of (a) $\text{Fe}_3\text{O}_4@\text{FSM-16}$, (b) $\text{Fe}_3\text{O}_4@\text{FSM-16-SO}_3\text{H}$ and (c) FSM-16.

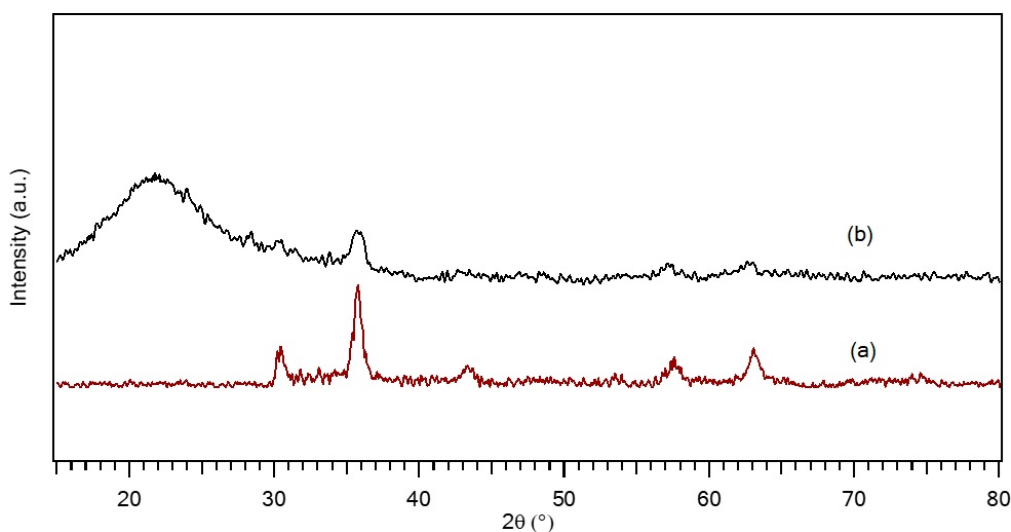


Fig. 5. High angle XRD patterns of (a) Fe_3O_4 , (b) $\text{Fe}_3\text{O}_4@FSM-16-SO_3H$.

Table 2. Textural properties of $\text{Fe}_3\text{O}_4@FSM-16$ and $\text{Fe}_3\text{O}_4@FSM-16-SO_3H$ Samples.

Entry	Catalyst	S_{BET} (m^2/g)	V_{pore} (cm^3/g)	D_{pore} (nm)
1	$\text{Fe}_3\text{O}_4@FSM-16$	842.7	1.024	4.86
2	$\text{Fe}_3\text{O}_4@FSM-16-SO_3H$	509.5	0.573	4.50

Fig. 6 shows the N_2 adsorption–desorption isotherms of the $\text{Fe}_3\text{O}_4@FSM-16$ and $\text{Fe}_3\text{O}_4@FSM-16-SO_3H$ samples. In both isotherms, a mesoporous inflection was observed at the medium p/p° partial pressure region ($p/p^\circ = 0.2 - 0.4$), owing to the capillary condensation of N_2 in the mesopores. A sharper hysteresis was seen at higher p/p° ($p/p^\circ > 0.7$). The hysteresis in this region is owing to the condensation of N_2 within the voids formed by nanoparticles.

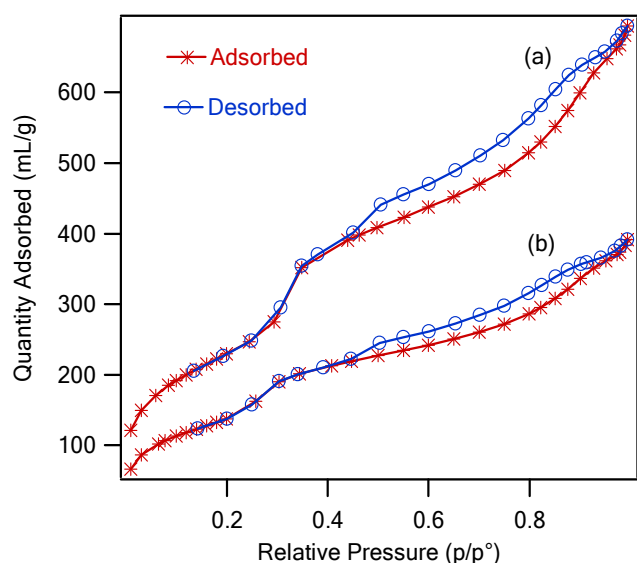


Fig. 6. N_2 adsorption–desorption isotherms of (a) $\text{Fe}_3\text{O}_4@FSM-16$, (b) $\text{Fe}_3\text{O}_4@FSM-16-SO_3H$.

FT-IR spectroscopy by means of pyridine absorption is a way to detect the distinction between Lewis and Brønsted acid sites of $\text{Fe}_3\text{O}_4@FSM-16-SO_3H$. Fig. 7 demonstrates the pyridine adsorbed spectrum of $\text{Fe}_3\text{O}_4@FSM-16-SO_3H$ was heated at disparate temperatures. The spectrum of pyridine adsorbed $\text{Fe}_3\text{O}_4@FSM-16$ displays only peaks of pyridine bonded Lewis acid sites at 1446 and 1598 cm^{-1} (Fig. 7b). The spectrum of pyridine adsorbed $\text{Fe}_3\text{O}_4@FSM-16-SO_3H$ before heat treatment (Fig. 7c) displays the contribution of the pyridine adducts in the region of $1400-1650$ cm^{-1} . The peak at 1487 cm^{-1} is ascribed to the combination of pyridine bonded to Lewis and Brønsted acid sites. The peaks appearing at 1537 cm^{-1} is due to Brønsted acid sites (pyridinium ion). The peak at 1610 cm^{-1} is assigned to the pyridine bonded Lewis acid sites of the catalyst. The peak at 1639 cm^{-1} in the spectrum of the catalyst before treatment with pyridine (Fig. 7a) is owing to the presence of water pending the preparation of the pellet sample. This sharp peak perhaps overlapped with another weak peak of the Brønsted acid sites at 1642 cm^{-1} . However, these results revealed the being of both Brønsted and Lewis acid sites on surface of the catalyst. As shown in Fig. 7b–e, with increasing the temperature, characteristic peaks of Lewis acid sites at 1610 cm^{-1} and peaks of Brønsted acid sites at 1537 cm^{-1} still remained. These results confirm that $-SO_3H$ functionalization has strengthened both Lewis and Brønsted acid sites on the surface of the catalyst.

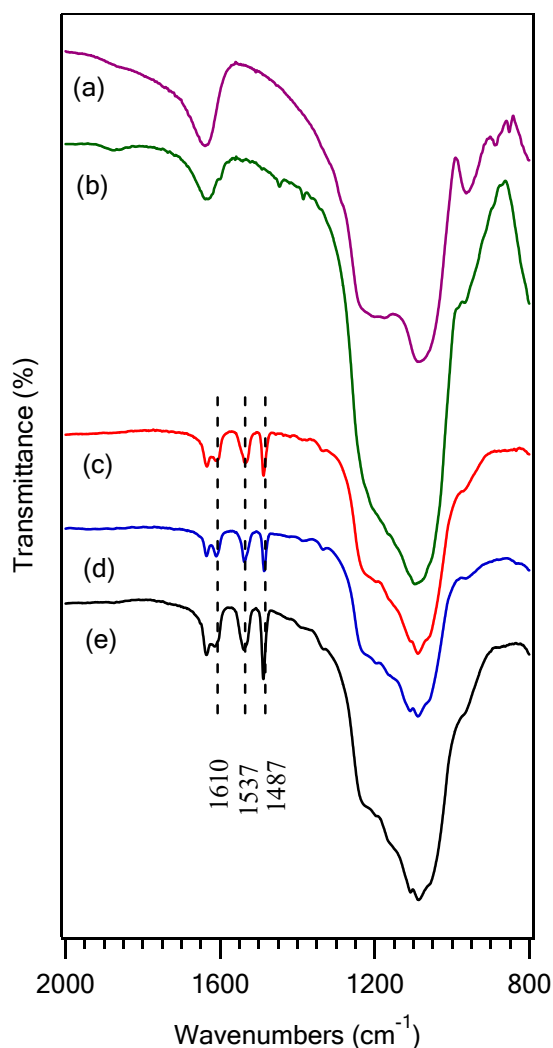


Fig. 7. FT-IR spectra of (a) $\text{Fe}_3\text{O}_4@\text{FSM-16-SO}_3\text{H}$, (b) pyridine adsorbed $\text{Fe}_3\text{O}_4@\text{FSM-16}$ and (c) $\text{Fe}_3\text{O}_4@\text{FSM-16-SO}_3\text{H}$ at ambient temperature and pyridine adsorbed $\text{Fe}_3\text{O}_4@\text{FSM-16-SO}_3\text{H}$ heated at (d) 100 °C, (e) 200 °C.

The catalyst acidity features that include the acidic strength and the total number of acid sites could be determined by potentiometric titration. Pursuant to this method, the initial electrode potential (E_i) shows the maximum acid strength of the surface sites [46]. Hence, a suspension of the magnetic catalyst in acetonitrile was potentiometrically titrated with a solution of 0.02 M *n*-butylamine. As shown in Fig. 8, $\text{Fe}_3\text{O}_4@\text{FSM-16-SO}_3\text{H}$ demonstrates higher strength than the bare support ($\text{Fe}_3\text{O}_4@\text{FSM-16}$).

To study the magnetic property of $\text{Fe}_3\text{O}_4@\text{FSM-16}$ and $\text{Fe}_3\text{O}_4@\text{FSM-16-SO}_3\text{H}$, magnetic measurements were performed using a room temperature VSM in an applied magnetic field. As shown in Fig. 9, typical super paramagnetic nature at 300 k is corroborated by not observing any hysteresis loops but also zero coercivity value for both samples.

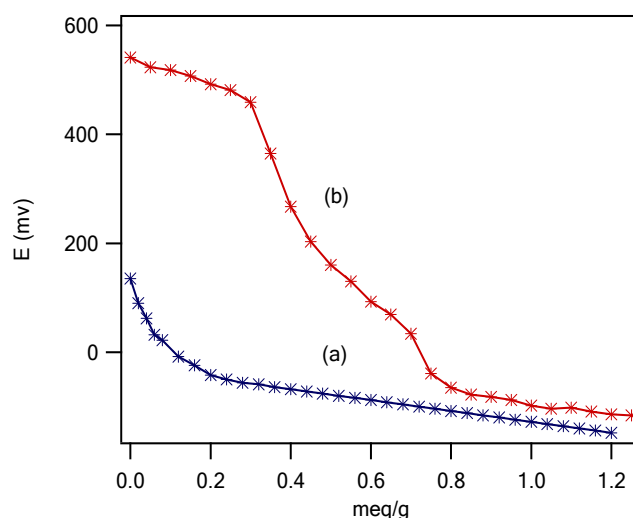


Fig. 8. Potentiometric titration of (a) $\text{Fe}_3\text{O}_4@\text{FSM-16}$ and (b) $\text{Fe}_3\text{O}_4@\text{FSM-16-SO}_3\text{H}$.

The saturation magnetization value of $\text{Fe}_3\text{O}_4@\text{FSM-16}$ and $\text{Fe}_3\text{O}_4@\text{FSM-16-SO}_3\text{H}$ are 4.30 emu/g and 1.25 emu/g (Fig. 9a and 9b), respectively. The observed decrease in magnetization saturation value after $\text{Fe}_3\text{O}_4@\text{FSM-16}$ modification is owing to the acidic environment needed for modification and the relative low mass ratio of Fe_3O_4 in the latter sample.

In addition, as seen in Fig. 10, the magnetic separation ability of the catalyst can be seen by putting a magnet near the reaction mixture balloons. The magnet attracts the magnetic nanoparticles towards itself, and when the external magnet is removed, the catalyst scatters in the solution with little shake (Fig. 10).

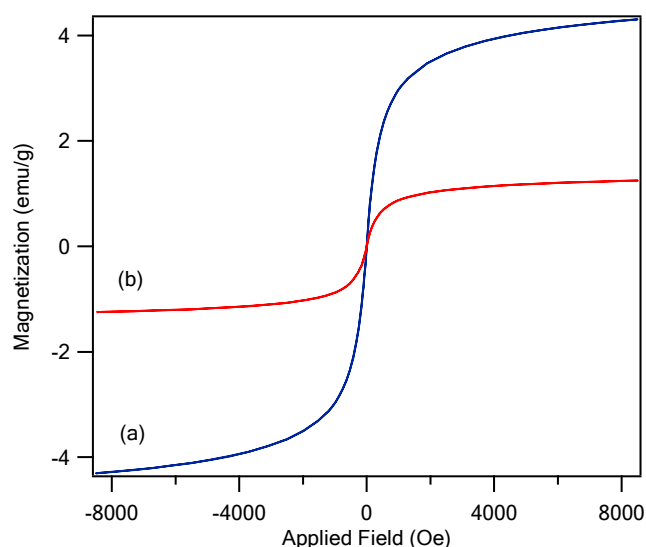


Fig. 9. Magnetization curves of (a) $\text{Fe}_3\text{O}_4@\text{FSM-16}$ and (b) $\text{Fe}_3\text{O}_4@\text{FSM-16-SO}_3\text{H}$.

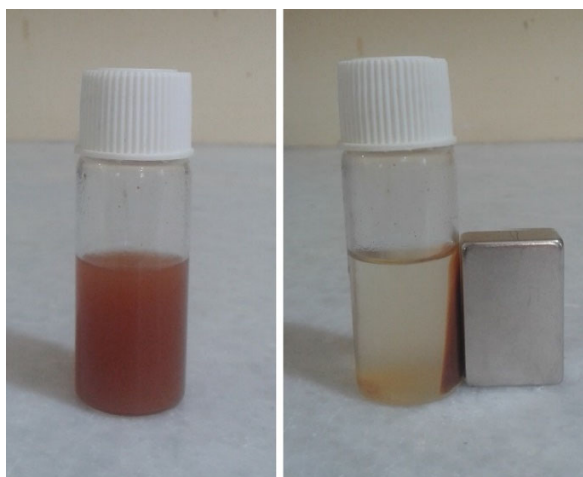


Fig. 10. Magnetic separation ability of $\text{Fe}_3\text{O}_4@\text{FSM-16-SO}_3\text{H}$.

3.2. Catalytic activity of $\text{Fe}_3\text{O}_4@\text{FSM-16-SO}_3\text{H}$

The catalytic activity of $\text{Fe}_3\text{O}_4@\text{FSM-16-SO}_3\text{H}$ was investigated in the multi-component reaction of benzaldehyde (1.1 mmol), malononitrile (1.1 mmol) and 3-methyl-1-phenyl-1H-pyrazol-5(4H)-one (1 mmol) as a model reaction for the synthesis of pyrano[2,3-*c*]pyrazole. The reaction was optimized for diverse

parameters such as the catalyst amount, temperature and solvent.

The effect of solvent and temperature was studied by doing the model reaction in the presence of 30 mg catalyst in various solvents and temperatures (Table 3, entries 1–8). Among them, the mixture of water and ethanol was selected as the best solvent at reflux conditions in terms of the yield of the product and reaction time (Table 3, entry 8). The lower yield and longer reaction time were achieved by the model reaction (synthesis of pyranopyrazole) in the presence of EtOH as the solvent at reflux and r.t. conditions (Table 3, entries 5, 6)

To optimize the required catalyst amount in the model reaction, diverse amounts of the catalyst were applied in the reaction and pursuant to the gained results (Table 3, entries 8, 13-15) 30 mg of the catalyst was found to be the best catalyst amount. Clearly, the $\text{Fe}_3\text{O}_4@\text{FSM-16}$ support strongly affected the efficiency of the heterogeneous catalyst. To show this, the model reaction was performed in the presence of 30 mg $\text{Fe}_3\text{O}_4@\text{FSM-16}$ under the same reaction conditions and lower yield of the product were obtained after 80 min (Table 3, entry 11).

Table 3. Optimization of the reaction conditions for the synthesis of pyrano[2,3-*c*]pyrazoles catalyzed by $\text{Fe}_3\text{O}_4@\text{FSM-16-SO}_3\text{H}$.^a

Entry	Catalyst	Catalyst amount (mg)	solvent	Time (min)	Yield (%) ^b
1	$\text{Fe}_3\text{O}_4@\text{FSM-16-SO}_3\text{H}$	30	CHCl_3	180	79
2	$\text{Fe}_3\text{O}_4@\text{FSM-16-SO}_3\text{H}$	30	CH_2Cl_2	300	76
3	$\text{Fe}_3\text{O}_4@\text{FSM-16-SO}_3\text{H}$	30	MeOH	45	85
4	$\text{Fe}_3\text{O}_4@\text{FSM-16-SO}_3\text{H}$	30	CH_3CN	55	81
5	$\text{Fe}_3\text{O}_4@\text{FSM-16-SO}_3\text{H}$	30	EtOH ^c	250	75
6	$\text{Fe}_3\text{O}_4@\text{FSM-16-SO}_3\text{H}$	30	EtOH	40	87
7	$\text{Fe}_3\text{O}_4@\text{FSM-16-SO}_3\text{H}$	30	Water	75	75
8	$\text{Fe}_3\text{O}_4@\text{FSM-16-SO}_3\text{H}$	30	EtOH/Water	30	89
9	$\text{Fe}_3\text{O}_4@\text{FSM-16-SO}_3\text{H}$	30	-	120 ^d	54
10	-	0	EtOH/Water	200	40
11	$\text{Fe}_3\text{O}_4@\text{FSM-16}$	30	EtOH/Water	80	79
12	FSM-16- SO_3H	30	EtOH/Water	55	79
13	$\text{Fe}_3\text{O}_4@\text{FSM-16-SO}_3\text{H}$	10	EtOH/Water	45	84
14	$\text{Fe}_3\text{O}_4@\text{FSM-16-SO}_3\text{H}$	20	EtOH/Water	40	89
15	$\text{Fe}_3\text{O}_4@\text{FSM-16-SO}_3\text{H}$	40	EtOH/Water	35	88

^aReactions were carried out under reflux condition with benzaldehyde (1.1 mmol), malononitrile (1.1 mmol) and 3-methyl-1-phenyl-1H-pyrazol-5(4H)-one (1 mmol).

^bIsolated yield.

^cReaction was carried out under r.t.

^dReaction was carried out at 80 °C.

The model reaction was also carried out in the presence of optimized amount of $\text{Fe}_3\text{O}_4@\text{FSM-16-SO}_3\text{H}$ under solvent-free conditions and the result shows the low yield of the product after 120 min (Table 3, entry 9). In the absence of the catalyst, the low yield of products after long reaction time was achieved (Table 3, entry 10). The model reaction in the presence of sulfonic acid functionalizing FSM-16 without magnetic core was carried out under optimized conditions and 79% yield of

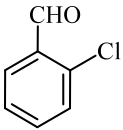
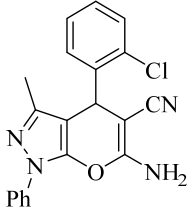
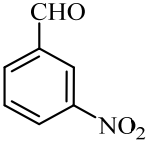
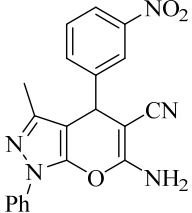
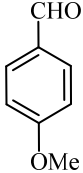
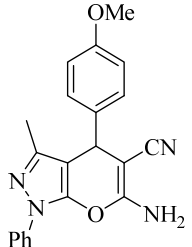
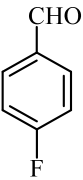
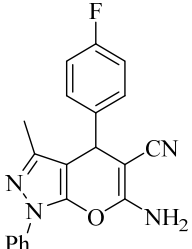
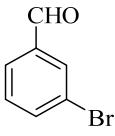
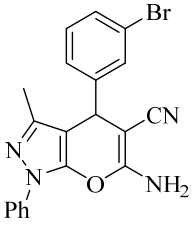
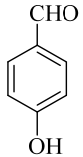
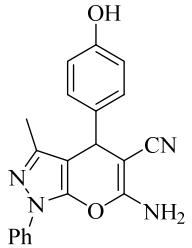
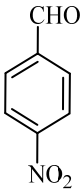
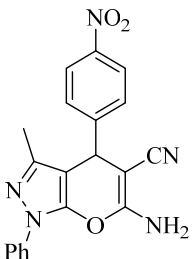
product was achieved after 55 min (Table 3, entry 12). Afterwards, the optimized reaction conditions were performed for the preparation of 1,4-dihydropyrano[2,3-c]pyrazoles using various aromatic aldehydes and the results are briefed in Table 4. It was found that this method is rather general for both, electron rich and electron poor aryl aldehydes and the corresponding products were obtained in good to excellent yields.

Table 4. Synthesis of pyrano[2,3-c]pyrazoles catalysed by $\text{Fe}_3\text{O}_4@\text{FSM-16-SO}_3\text{H}$.

Reaction scheme: Benzaldehyde (1) + 1-phenyl-2-methyl-5-oxo-1H-imidazole (2) + malononitrile (3) $\xrightarrow[\text{EtOH/Water, Reflux}]{\text{Fe}_3\text{O}_4@\text{FSM-16-SO}_3\text{H (30 mg)}}$ 1,4-dihydropyrano[2,3-c]pyrazole (4)

Entry	Aldehyde (1)	Pyrano[2,3-c]pyrazole (4)	Time (min)	Yield (%) ^a	m.p. (°C)		Ref.
					Found	Reported	
a			30	89	178-179	172-174	[40]
b			25	81	180-182	178-180	[40]
c			40	89	176-178	175-177	[40]
d			20	85	155-158	158-160	[37]

Table 4. (Continued).

e			50	83	147-149	145-146	[47]
f			15	82	187-189	190-191	[40]
g			80	79	170-171	172-173	[40]
h			15	80	171-173	175-177	[40]
i			20	86	167-169	160-161	[40]
j			45	80	216-217	213-214	[40]
k			20	84	195-198	192-194	[40]

^aIsolated yield.

To demonstrate the reusability of $\text{Fe}_3\text{O}_4@\text{FSM-16-SO}_3\text{H}$, it was separated from the reaction mixture and washed with ethanol. The catalyst was dried and activated in an oven at $120\text{ }^\circ\text{C}$ for 2 h. The recycled catalyst was applied in a model reaction under optimized conditions and results were summarized in Table 5. The catalyst was found to be reusable for at least 3 cycles without notable loss of activity (Table 5).

A plausible mechanism for the synthesis of pyrano[2,3-c]pyrazoles in the presence of $\text{Fe}_3\text{O}_4@\text{FSM-16-SO}_3\text{H}$ is illustrated in Scheme 3.

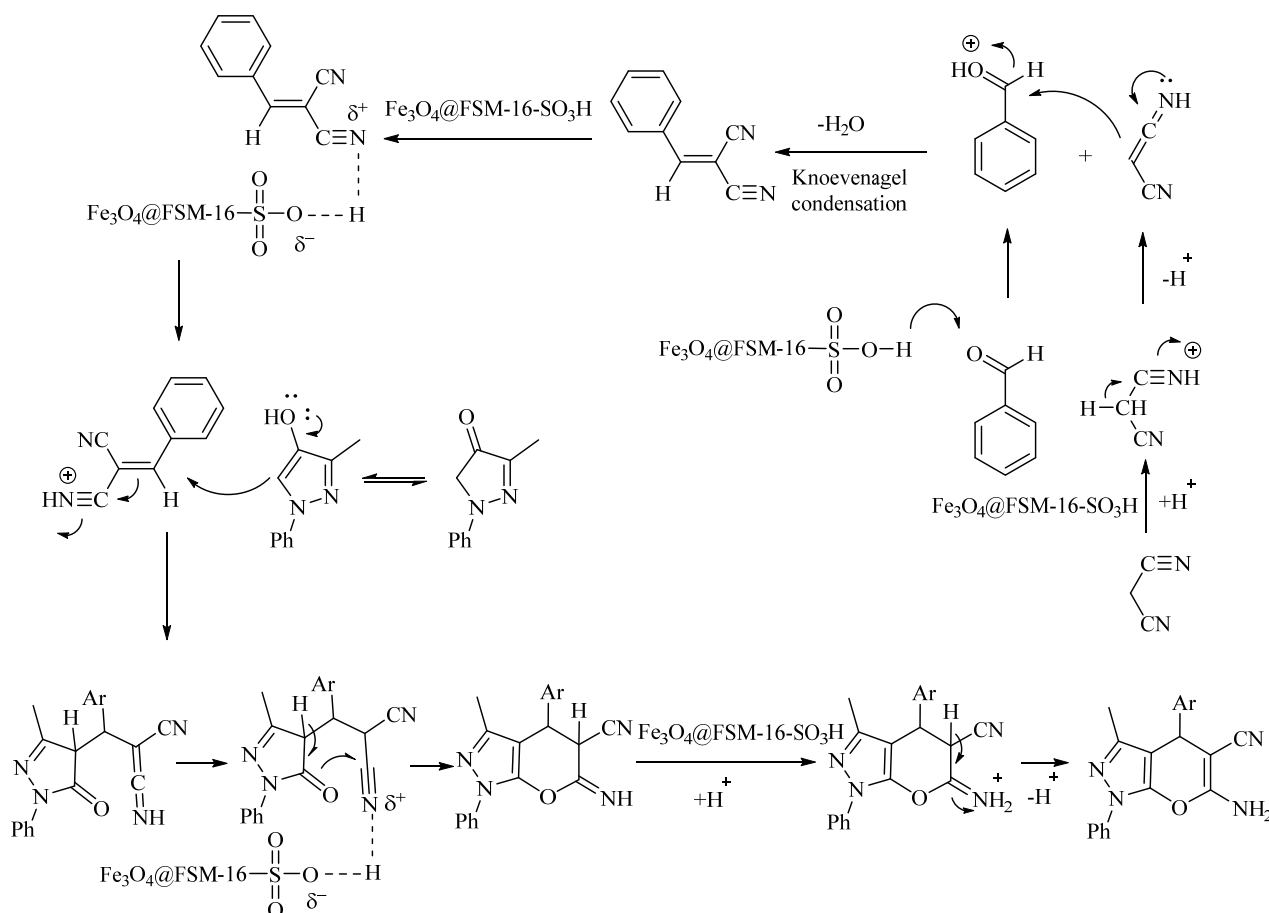
Table 6 shows the comparison between the activity of the $\text{Fe}_3\text{O}_4@\text{FSM-16-SO}_3\text{H}$ and other reported catalysts for the pyrano[2,3-c]pyrazoles synthesis through the reaction of benzaldehyde, malononitrile and 3-methyl-1-phenyl-1H-pyrazol-5(4H)-one. Results show that $\text{Fe}_3\text{O}_4@\text{FSM-16-SO}_3\text{H}$ is comparable with other catalytic systems in term of the yield and/or reaction time. In addition to this, easy work-up and using a reusable catalyst are other benefits of this method.

Table 5. Recycling of $\text{Fe}_3\text{O}_4@\text{FSM-16-SO}_3\text{H}$ nanoparticles.

Run	Yield (%)	Time
1	89	30
2	88	35
3	84	45

4. Conclusions

In summary, we have developed a novel, mild, and efficient strategy for the synthesis of pyrano[2,3-c]pyrazoles from aryl aldehydes, malononitrile and 3-methyl-1-phenyl-1H-pyrazol-5(4H)-one using $\text{Fe}_3\text{O}_4@\text{FSM-16-SO}_3\text{H}$ as a magnetite recoverable heterogeneous catalyst. This magnetic nano catalyst can be easily separated from the reaction mixture by an external magnet. The catalyst was prepared and characterized by FESEM, BET, XRD, pyridine absorption, potentiometric titration and FT-IR techniques. The results show that mesoporous structure of the bare support ($\text{Fe}_3\text{O}_4@\text{FSM-16}$) was maintained during chlorosulfonic acid treatment. The methodology is simple, rapid, and relatively inexpensive can afford good to excellent yields with operational simplicity.



Scheme 3. A plausible mechanism for the synthesis of pyrano[2,3-c]pyrazoles in the presence of $\text{Fe}_3\text{O}_4@\text{FSM-16-SO}_3\text{H}$.

Table 6. The comparative study of the activity of Fe₃O₄@FSM-16-SO₃H with other catalysts.

Entry	Catalyst	Solvent	Temp (°C)	Time (min)	Yield ^a	Ref.
1	Fe ₃ O ₄ @FSM-16-SO ₃ H	Ethanol/water	Reflux	30	89	This work
2	DBSA (10 mol%)	Water	60	180	88	[37]
3	H ₁₄ [NaP ₅ W ₃₀ O ₁₁₀]	Ethanol	Reflux	60	84	[41]
4	HTMAB	Water	85-90	180	89	[39]
5	TEBA	Water	90	360	99	[38]
6	[Sipim]HSO ₄	Solvent free	110	90	92	[48]
7	NH ₄ H ₂ PO ₄ /Al ₂ O ₃	Ethanol	Reflux	15	84	[49]
8	Sulfamic acid	Ethanol	Reflux	600	82	[50]
9	-	Ethanol/water	100	150	88	[51]

^aIsolated yield

Acknowledgements

We are thankful to the Yazd University Research Council for partial support of this work.

References

- [1] O. Veisheh, C. Sun, J. Gunn, N. Kohler, P. Gabikian, D. Lee, N. Bhattarai, R. Ellenbogen, R. Sze, A. Hallahan, *Nano Lett.* 5 (2005) 1003-1008.
- [2] A.H. Latham, A.N. Tarpara, M.E. Williams, *Anal. Chem.* 79 (2007) 5746-5752.
- [3] N. Shamim, L. Hong, K. Hidajat, M. Uddin, *Sep. Purif. Technol.* 53 (2007) 164-170.
- [4] B. Gilbert, J.E. Katz, J.D. Denlinger, Y. Yin, R. Falcone, G.A. Waychunas, *J. Phys. Chem. C* 114 (2010) 21994-22001.
- [5] X. Zhou, Y. Shi, L. Ren, S. Bao, Y. Han, S. Wu, H. Zhang, L. Zhong, Q. Zhang, *J. Solid State Chem.* 196 (2012) 138-144.
- [6] Y. Guan, C. Jiang, C. Hu, L. Jia, *Talanta* 83 (2010) 337-343.
- [7] Y. Arum, Y. Song, J. Oh, *Appl. Nanosci.* 1 (2011) 237-246.
- [8] J. Wang, S. Zheng, Y. Shao, J. Liu, Z. Xu, D. Zhu, *J. Colloid Interface Sci.* 349 (2010) 293-299.
- [9] P. Lu, J.-L. Zhang, Y.-L. Liu, D.-H. Sun, G.-X. Liu, G.-Y. Hong, J.-Z. Ni, *Talanta* 82 (2010) 450-457.
- [10] S. Rostamnia, E. Doustkhah, *J. Magn. Magn. Mater.* 386 (2015) 111-116.
- [11] A. Shoshi, J. Schotter, P. Schroeder, M. Milnera, P. Ertl, R. Heer, G. Reiss, H. Brueckl, *Biosens. Bioelectron.* 40 (2013) 82-88.
- [12] Y. Yao, S. Miao, S. Yu, L.P. Ma, H. Sun, S. Wang, *J. Colloid Interface Sci.* 379 (2012) 20-26.
- [13] G.G. Utkan, F. Sayar, P. Batat, S. Ide, M. Kriechbaum, E. Pişkin, *J. Colloid Interface Sci.* 353 (2011) 372-379.
- [14] N. Mizutani, T. Iwasaki, S. Watano, T. Yanagida, H. Tanaka, T. Kawai, *Bull. Mater. Sci.* 31 (2008) 713-717.
- [15] S. Rostamizadeh, N. Shadjou, M. Azad, N. Jalali, *Catal. Commun.* 26 (2012) 218-224.
- [16] F. Zhang, J. Jin, X. Zhong, S. Li, J. Niu, R. Li, J. Ma, *Green Chem.* 13 (2011) 1238-1243.
- [17] N. Gharibpour, M. Abdollahi-Alibeik, A. Moaddeli, *ChemistrySelect* 2 (2017) 3137-3146.
- [18] M. Abdollahi-Alibeik, A. Rezaeipoor-Anari, *J. Magn. Magn. Mater.* 398 (2016) 205-214.
- [19] A. Moaddeli, M. Abdollahi-Alibeik, *J. Porous Mater.* (2017).
- [20] H.H. Yiu, M. Keane, Z.A. Lethbridge, M.R. Lees, A.J. El Haj, J. Dobson, *Nanotechnology* 19 (2008) 255606-255612.
- [21] T. Yanagisawa, T. Shimizu, K. Kuroda, C. Kato, *Bull. Chem. Soc. Jpn.* 63 (1990) 988-992.
- [22] S. Inagaki, Y. Fukushima, K. Kuroda, *J. Chem. Soc. Chem. Commun.* (1993) 680-682.
- [23] S. Inagaki, A. Koiwai, N. Suzuki, Y. Fukushima, K. Kuroda, *Bull. Chem. Soc. Jpn.* 69 (1996) 1449-1457.
- [24] Y. Sakamoto, S. Inagaki, T. Ohsuna, N. Ohnishi, Y. Fukushima, Y. Nozue, O. Terasaki, *Microporous Mesoporous Mater.* 21 (1998) 589-596.
- [25] K. Bachari, A. Touileb, A. Saadi, D. Halliche, O. Cherifi, *J. Porous Mater.* 17 (2010) 573-581.
- [26] S.-I. Matsuura, T. Itoh, R. Ishii, T. Tsunoda, K. Sakaguchi, T. Hanaoka, F. Mizukami, *Microporous Mesoporous Mater.* 131 (2010) 245-251.
- [27] T. Selvam, M. Köstner, G.T.P. Mabande, W. Schwieger, N. Pfänder, R. Schlögl, *J. Porous Mater.* 14 (2007) 263-272.
- [28] C.-Y. Chen, S.-Q. Xiao, M.E. Davis, *Microporous Mater.* 4 (1995) 1-20.
- [29] T. Yamamoto, T. Tanaka, T. Funabiki, S. Yoshida, *J. Phys. Chem. B* 102 (1998) 5830-5839.
- [30] T. Yamamoto, T. Tanaka, S. Inagaki, T. Funabiki, S. Yoshida, *J. Phys. Chem. B* 103 (1999) 6450-6456.
- [31] M.E. Zaki, H.A. Soliman, O.A. Hiekal, A.E. Rashad, *Z. Naturforsch., C: J. Biosci.* 61 (2006) 1-5.
- [32] P.W. Smith, S.L. Sollis, P.D. Howes, P.C. Cherry, I.D. Starkey, K.N. Cogley, H. Weston, J. Scicinski, A. Merritt, A. Whittington, *J. Med. Chem.* 41 (1998) 787-797.
- [33] M. Zaki, E. Morsy, F. Abdel-Motti, F. Abdel-Megeid, *Heterocycl. Commun.* 10 (2004) 97-102.

- [34] N. Foloppe, L.M. Fisher, R. Howes, A. Potter, A.G. Robertson, A.E. Surgenor, *Bioorg. Med. Chem.* 14 (2006) 4792-4802.
- [35] H. Junek, H. Aigner, *Chem. Ber.* 106 (1973) 914-921.
- [36] H. Wamhoff, E. Kroth, C. Strauch, *Synthesis* (1993) 1129-1132.
- [37] T.-S. Jin, R.-Q. Zhao, T.-S. Li, *Arkivoc* XI (2006) 176-182.
- [38] D. Shi, J. Mou, Q. Zhuang, L. Niu, N. Wu, X. Wang, *Synth. Commun.* 34 (2004) 4557-4563.
- [39] T.S. Jin, A.Q. Wang, Z.L. Cheng, J.S. Zhang, T.S. Li, *Synth. Commun.* 35 (2005) 137-143.
- [40] M. Abdollahi-Alibeik, A. Moaddeli, K. Masoomi, *RSC Adv.* 5 (2015) 74932-74939.
- [41] M. Heravi, A. Ghods, F. Derikvand, K. Bakhtiari, F. Bamoharram, *J. Iran. Chem. Soc.* 7 (2010) 615-620.
- [42] H. Sheibani, M. Babaie, *Synth. Commun.* 40 (2009) 257-265.
- [43] Z. Ren, W. Cao, W. Tong, Z. Jin, *Synth. Commun.* 35 (2005) 2509-2513.
- [44] S. Ghosh, A. Badruddoza, M. Uddin, K. Hidajat, *J. Colloid Interface Sci.* 354 (2011) 483-492.
- [45] H. Araki, A. Fukuoka, Y. Sakamoto, S. Inagaki, N. Sugimoto, Y. Fukushima, M. Ichikawa, *J. Mol. Catal. A: Chem.* 199 (2003) 95-102.
- [46] L.R. Pizzio, P.G. Vázquez, C.V. Cáceres, M.N. Blanco, *Appl. Catal. A* 256 (2003) 125-139.
- [47] M. Farahi, B. Karami, I. Sedighimehr, H.M. Tanuraghaj, *Chin. Chem. Lett.* 25 (2014) 1580-1582.
- [48] K. Niknam, A. Piran, *Green Sustainable Chem.* 3 (2013) 1-8.
- [49] B. Maleki, S.S. Ashrafi, *RSC Adv.* 4 (2014) 42873-42891.
- [50] S.V. Shinde, W.N. Jadhav, J.M. Kondre, S.V. Gampawar, N.N. Karade, *J. Chem. Res.* 2008 (2008) 278-279.
- [51] S.R. Mandha, S. Siliveri, M. Alla, V.R. Bommena, M.R. Bommineni, S. Balasubramanian, *Bioorg. Med. Chem. Lett.* 22 (2012) 5272-5278.